

INCREASING THE FUNCTIONAL SERVICE LIFE OF POROUS SURFACINGS: DEVELOPMENT OF TEST METHODS TO STUDY THE EFFECT OF REJUVENATING BINDERS**Peer Reviewed****Martin van de Ven, Jian Qiu, Yuan Zhang**

Delft University of Technology, The Netherlands (m.f.c.vandeven@tudelft.nl)

Abstract

Traffic noise is becoming a major concern in the more densely populated areas in Europe. Noise reducing porous surfacings are considered one of the few viable possible contributors to solve this problem and are used in large quantities in Western Europe. Unfortunately these surfacings have a limited functional service life due to the problem of ravelling, (defined in this paper as stone loss at the surface. To improve the service life of these layers binders are applied at the surface with a rejuvenating component. The impact on the volumetric composition of the porous surfacings was investigated with CT scans and optical thin section microscopy at meso and micro level. Mechanical properties were tested with a nano indenter at the level of the mastic, a beam test at the level of the material and at the surface layer an abrasion ravelling test was applied. The influence on chemical composition was studied with FTIR and GPC. For a number of tests the development of the test method or interpretation is shown. Results are given from CT scans, nano indentation, bending beam and FTIR. It was shown that the three binders used in this project have different characteristics when placed on the porous surface.

1. INTRODUCTION

In the search for long life asphalt pavements, some even talk about perpetual pavements, many important developments can be reported from the structural point of view. Important aspects related to long term structural performance like (self)healing, high stiffness base mixtures (EME), endurance limit, polymer modified base mixtures with long fatigue lives, etcetera, are making their impact on the flexible pavement design methods.

However, pavement structures designed for long structural lives, also need to satisfy functional requirements at the pavement surface like skid resistance (safety) and acceptable traffic noise (annoyance). Especially traffic noise is becoming a major concern in the more densely populated areas in Europe. Noise reducing porous surfacings are considered one of the few viable possible contributors to solve this problem and are used in large quantities in Western Europe.

Unfortunately most of these surfacings have a limited functional service life due to the problem of ravelling, defined as stone loss at the surface. To improve the service life of these layers and in this way also contribute to long life pavements, preventive maintenance methods are under development for these layers. At Delft University of Technology some promising build-in self healing methods are investigated at the moment, like addition of steelwool or capsules containing rejuvenator to the porous mixture, which can be activated. However, the most promising method at the moment is the addition of new binders at the surface with a rejuvenating component. In this paper the test methods which were developed to investigate the working of the rejuvenating binder are described and discussed. It will also be shown that different binders and application techniques influence the distribution of the binder in the porous layer.

2. TEST SECTIONS, REJUVENATORS AND TESTING PROGRAM

Two test sections on two Dutch motorways (A50 and A73) with heavy traffic were treated with rejuvenating binders in 2010. Both test sections were 5 years in service and still in good condition when the rejuvenators were applied. The wearing course of the A50 motorway (located from 190.7 km to 192.7 km) is a Dutch single-layer porous asphalt (PA) 0/16 means grading with maximum grain size 16 mm. The bituminous binder in this section was a Penetration 70/100 bitumen with 5.2 by weight in the mixture. The wearing course of the A73 motorway (between 100.1 km to 101.5 km) is a Dutch two-layer porous asphalt consisting of a 25 mm top layer of PA 4/8 and a 45 mm bottom layer of PA 11/16. The bituminous binder in the top layer of this section is an SBS modified bitumen.

Three rejuvenation products were supplied by three contractors. Binder E is a bitumen emulsion, which was sprayed on the pavement at ambient temperature. Binder B is a bituminous polymer modified binder, which was sprayed on the pavement at a temperature of 180°C. Binder H, sprayed at a temperature of 70°C, is also bitumen emulsion, which was blown in after application with hot air. Small crushed sand or glass particles were sprayed on the pavement after the application of rejuvenators in order to increase the skid resistance. Cores with a diameter of 150 mm were drilled from the test sections on the pavement for laboratory testing. Specimens from the reference wearing course (without treatment) were also taken for comparison.

The aim of the testing program was to find out if the addition of the new binder could be observed and if the new binder had impact on the behaviour of the porous layer, with the focus on increasing ravelling resistance. An overview of the testing program divided in a volumetric, mechanical, chemical and functional part is given in figure 1 .

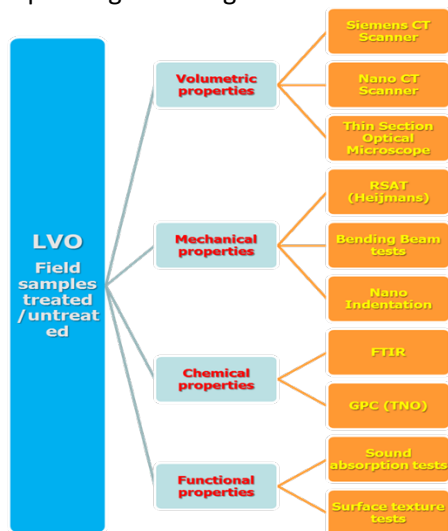


Figure 1. Overview of the testing program on cores taken from the reference and treated porous surfacings.

In figure 2 a flow chart is given for the test samples and how they were used for the different tests. In all cases the 150 mm diameter cores taken from the field were scanned in a large CT scanner to obtain the bulk volumetrics. In case of functional tests, also absorption and texture were measured on the 150 mm diameter cores. These tests are not reported in this paper.

Beams were sawn from the centre of the porous asphalt cores from motorways A50 and A73. Figure 3 shows how a beam and a small core were taken from a large core. For the single layer porous asphalt (SLPA) the beam dimension were 150 mm in length, 50 mm in width and 40 mm in height. For the two layer porous asphalt (TLPA) beams the height was 25 mm.

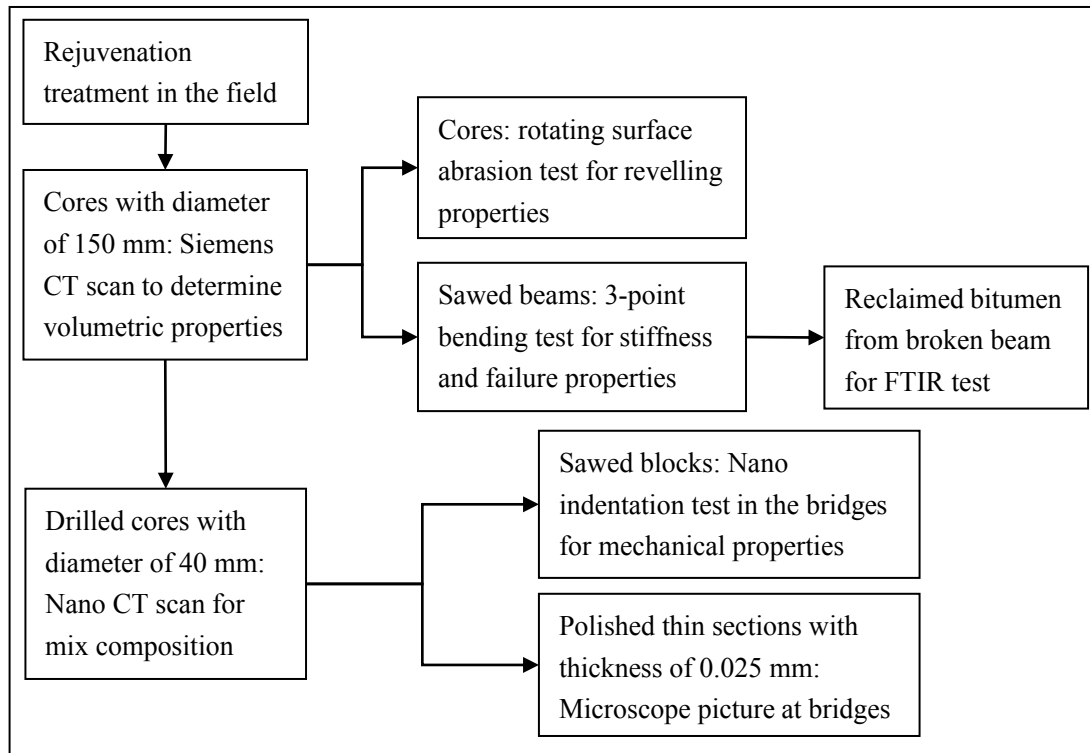


Figure 2. Flow chart for the material preparation related to the different tests.

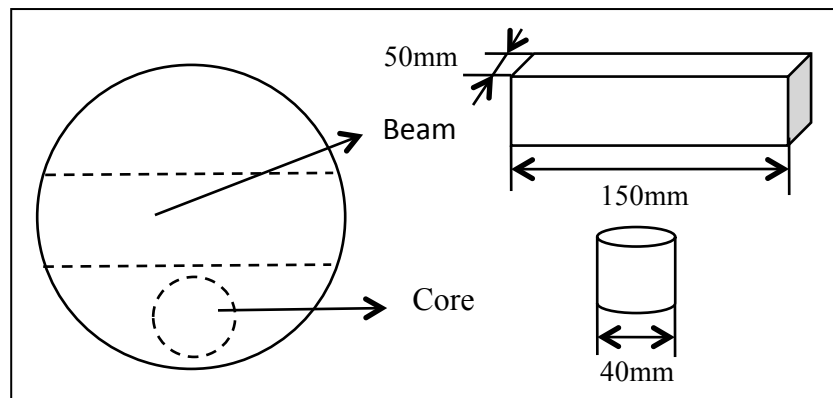


Figure 3: Example of the beam and the small core from a large 150 mm core

3. DEVELOPMENT OF TEST METHODS

Several test methods were developed specific for this research. The development of the tests and the way of interpretation are given in three appendices at the end of the paper for the interested reader. The volumetric tests are discussed and explained in appendix 1. This group contains Computer Tomography (CT) scans (A1.1) on complete 150 mm diameter cores, nano CT scans on 40 mm diameter cores and thin section microscope pictures (A1.2).

In appendix 2 the tests for mechanical properties are described. With a nano indenter the stiffness of the mortar is measured (A2.1), with the bending beam test the stiffness and strength of the mixture (A2.2) and with the RSAT the ravelling at the surface of the porous asphalt is estimated (A2.3).

The chemical properties are investigated with FTIR and GPC. In this paper only the test set up and results for the FTIR measurements are reported. In appendix 3 the development of the recovery test (A3.1) and the way to perform the FTIR test in this specific case (A3.2) are described.

4. TEST RESULTS

4.1 Results CT scans [1, 6]

An example of the distribution of the different components is given in figure 4. It shows the distribution of the voids etc. over the height of the core. Clogged material in the cores probably has a similar density as the mortar and is added to the mortar. Some sand particles in the mortar are of the same rock material as the aggregate (Bestone). Based on their density these sand size particles are added to the rock part and not to the mortar. Figure 4 shows the distribution of the air voids of the top 10mm of porous asphalt from all the sections. It shows that the new binders do not influence the volumetric properties.

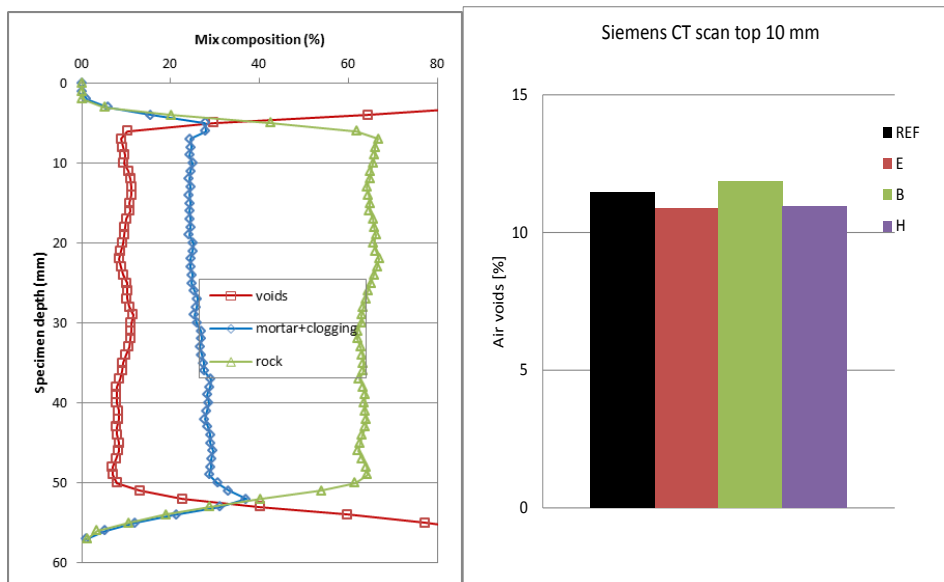


Figure 4. Left: Example of distributions of voids, mortar and aggregate over the height of the sample from Siemens CT scans, Right: Distribution of air voids top 10 mm of porous asphalt from Siemens CT scans

From the nano CT scan test, two types of typical two-dimensional X-ray images have been found both in the top and front views of samples. In figure 5 the top image shows three components: the highest grayscale (light) parts represent rock in the cores; the lowest grayscale (black) parts represent voids in the cores; intermediate parts represent mortar and clogging. For some treated sections, another type of image containing four components was found as shown in the bottom image. Different parts can be seen around voids of cores with a clear grayscale between that of voids and mortar. They have a higher grayscale than voids and a lower grayscale than mortar and clogging. This material is coloured red in figure 5.

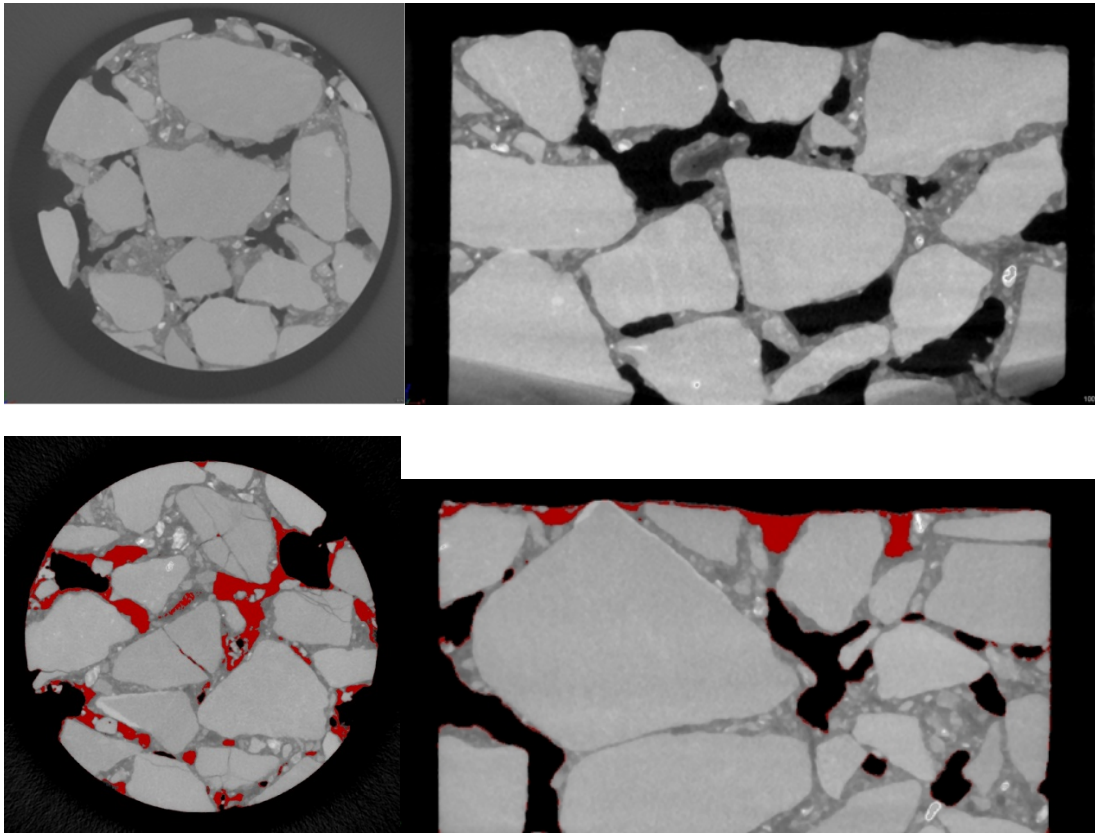


Figure 5. Typical top and front views of the core samples with three compositions (top) and four compositions with new binder in red (bottom).

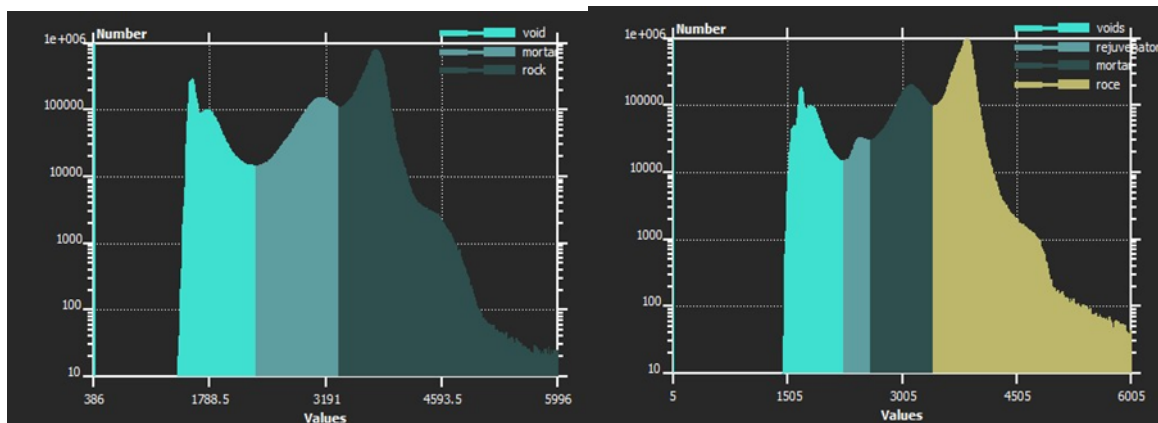


Figure 6. Histogram of grayscale of samples with three composition (left) and four composition (right)

It is remarkable that images with four components can be found in the samples treated with new binder. No images with four components were found in the reference samples, see figure 6 at the left.

So the fourth composition which is a kind of homogeneous material as seen in figure 6 at the right may be defined as the new added binder. From the grey values in the histograms a clear peak can be detected shortly before the peak of the mortar on both the treated sections from B and H. The histograms from the E section show no separate peak related to LVO binder. The binder of the B section

is visible to a depth of about 8-10mm. The binder of the H section is visible over the whole scanned height.

4.2 Results thin sections microscopy [2, 7]

An example of a microscope picture of the thin sections is given in figure 7. The thin section of a porous asphalt core with new binder shows stone parts (gray), mortar parts (black) and epoxy resin parts (yellow). The epoxy resin was used to fill all the voids and cracks in the cores to avoid damage during the sawing and polishing process. The microscope picture was taken from an observation point at the top of the porous asphalt core. It is very clear in this microscope picture that the fresh binder can be separated from the aged mortar. This information is used to investigate the distribution of the new binder in the porous asphalt core.

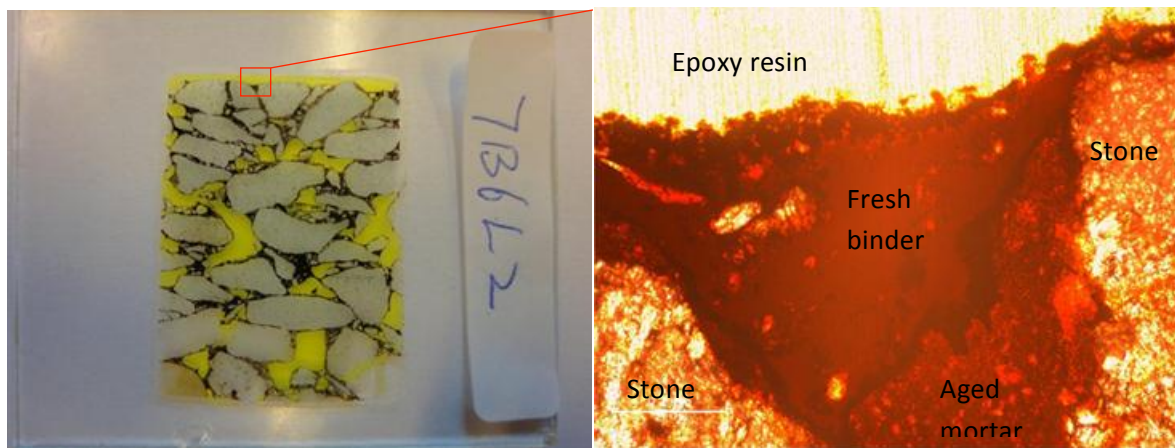


Figure 7. The thin section (left) of a porous asphalt core with new binder and the picture of an observation point (right) under microscope

All microscope pictures are reported in [2,6]. It is impossible to discuss them in this paper. The microscope pictures were used to confirm certain trends or to support measurements with other tests.

4.3 Results from nano indentation [3, 8]

Figure 8 shows a microscope image and indenter locations of sample B7L3. A new layer can be seen in the old mortar. It seems that a crack within the old mortar is filled with new binder. The testing locations in this new layer (points 3-8) show a very low indentation modulus of 0.36 GPa. As there is no such low indentation modulus in reference samples, this new layer with lower indentation modulus must be new binder. Figure 9 shows how the indentation modulus changes with depth for samples H13T1 and H10 L2. The minimum indentation modulus of the reference sample H10 L2 is 1.463 GPa. However, the minimum indentation modulus of the treated sample H13T1 is much lower. The lower modulus of this region is caused by new binder. As discussed previously, new layers of binder can be seen above or within the mortar in the samples from B sections and H sections. The indentation modulus of these new binder layers is much lower than the modulus of old mortar. For the samples from E sections, no new binder layer can be seen with the microscope when determining the testing locations. However, much more locations in the E section samples show lower indentation modulus than the reference samples. The average indentation moduli of the mortar in reference samples and treated samples are summarized in table 1 (the modulus of sand and new binder in the mortar are excluded). As shown in table 1, the indentation modulus of the mortar in reference section samples is higher than that of all three treated

sections. It means that all 3 new binders are capable of softening the mortar in porous asphalt. Besides, the indentation modulus of the mortar in the samples from E sections is lowest, there is no new binder visible in the sample. One possible explanation is that most of this binder is rejuvenator penetrating almost completely into the old mortar.

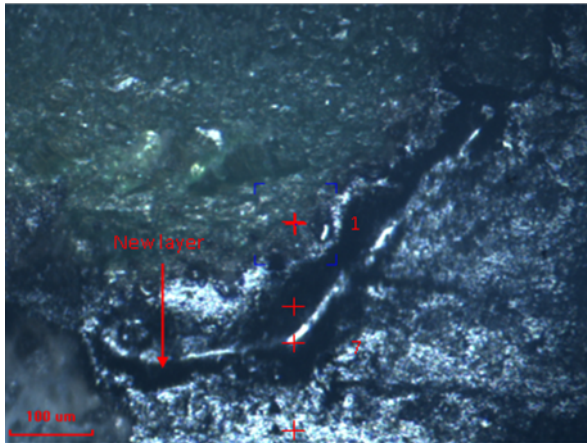


Figure 8. Microscope image and indenter locations

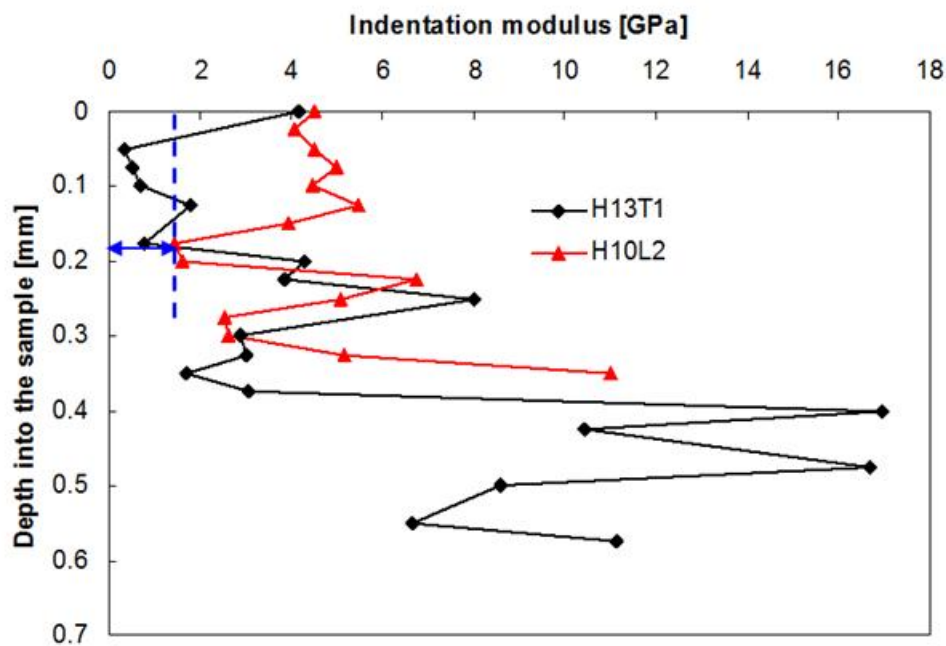


Figure 9. Indentation modulus changes in sample H13T1 (treated) and H10 L2 (reference)

Table 1. Indentation modulus of mortar in reference samples and treated samples

Sample	Number of measurement	Indentation modulus of mortar
Reference sections	98	2.85 GPa
E sections	117	2.10 GPa
B sections	62	2.18 GPa
H sections	53	2.22 GPa

4.4 Bending beam test results [4, 9]

4.4.1. Stiffness

The average values of bending stiffness in surface-down and surface-up mode of SLPA beams are shown in figure 10. These results are calculated from 10 reference beams, 6 treated beams with binder E, 2 treated beams with binder B and 4 treated beams with binder H.

The bending stiffness increases with increasing loading frequency. Both in the surface-down and surface-up mode, the treated beams show a higher bending stiffness. The beams with binder B show the highest bending stiffness in the SLPA sections. Binder B is a hot applied modified binder and only distributed in the top part. This could result in a strong bond between the aggregates at the surface. The bending stiffness in the surface-up mode is mostly higher than in the surface-down mode. One explanation can be that the surface has much more macro-texture than the sawn area.

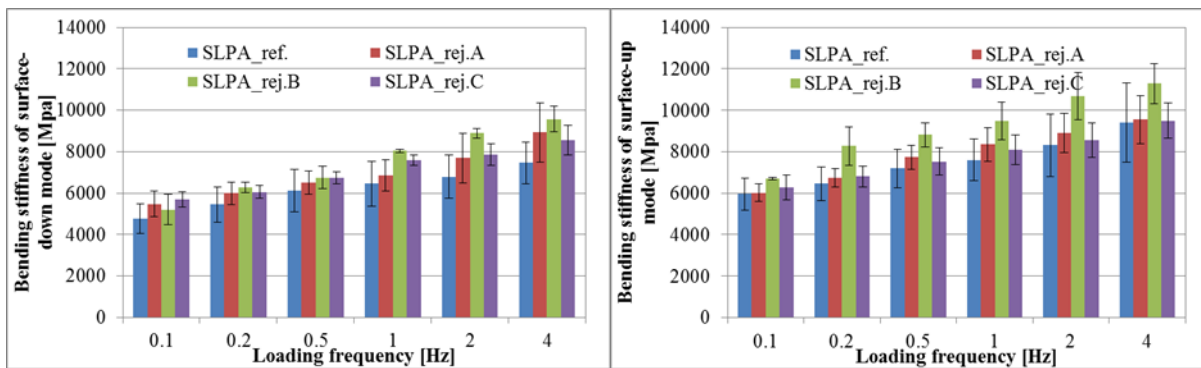


Figure 10. Average of bending stiffness in surface-down and surface-up mode of SLPA beams

Figure 11 shows the average values of bending stiffness of TLPA beams. For binder B only one beam was available for testing. For the other sections, the results of two beams were used for calculating the average value. In the surface-down mode of TLPA sections, the reference beams show a lower bending stiffness than treated beams with binder A (E) and C (H). Generally the TLPA beams show a higher stiffness than the SLPA beams in this research.

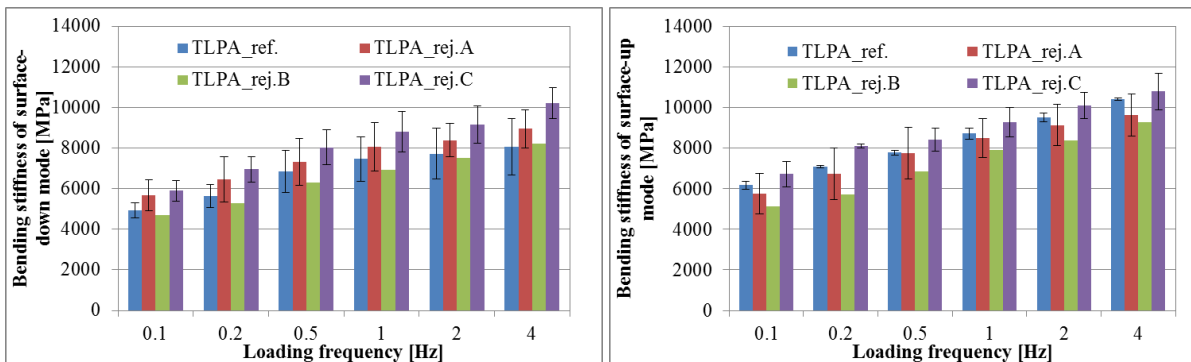


Figure 11. Average of bending stiffness in surface-down and surface-up mode of TLPA beams

4.4.2 Tensile strength

After the stiffness tests, the failure properties of beams were tested in a constant vertical displacement rate test. The load versus deflection curves are used to calculate the properties. A typical loading curve is shown in Figure 12. As shown in figure 12 the original loading curve with some noise is plotted to get a smooth curve. The peak of the plotted curve is defined to calculate the tensile strength at the bottom of the beam. The area under the curve of the load versus deflection represents the failure energy. During the initial loading period, the load and deflection show linear behaviour and can be used to calculate an initial modulus of the beam. The slope of the linear relationship between the load and deflection is used as follows:

$$E_{initial} = \frac{PL^3}{4\delta WH^3} \quad (2)$$

Where, $E_{initial}$ is the initial modulus of test beam, P is the concentrated load, δ is the deflection, L is the support span of test beam, W is the width and H is the height. Average values and a standard deviation of failure properties for the beams from A50 are given in Table 2. The average bending strength of all the beams is approximate 4 MPa. That means this single-layer porous asphalt (A50) is still in good condition. For A73 it can be seen from table 3 that the bending strength is lower compared to the values of A50. It is important to keep in mind that the height of these beams were considerably lower.

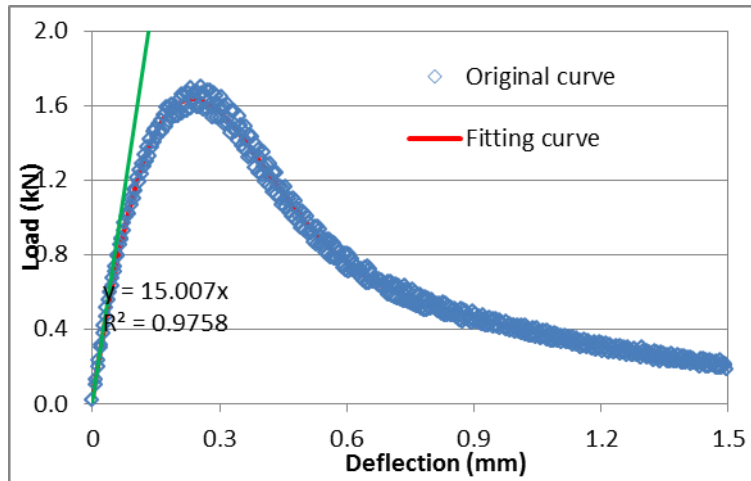


Figure 12. A typical loading curve in the failure test

Table 2. Failure properties for the beams from A50 (5°C, 0.01mm/s)

Section	Amount of specimens	Max stress (MPa)	Strain at max load	Initial modulus (MPa)	Energy until max load (mJ)	Energy until deflection-1.5mm (mJ)
A50-R	10	4.09 (0.56)	3.8E-03 (6.2E-04)	2675 (419)	318 (89)	1054 (229)
A50-P1	6	4.04 (0.33)	3.9E-03 (6.4E-04)	2438 (245)	310 (71)	1110 (132)
A50-P2	3	4.12 (0.13)	3.4E-03 (4.6E-04)	1986 (69)	261 (43)	911 (120)
A50-P3	5	4.10 (0.16)	4.0E-03 (4.2E-04)	2648 (216)	323 (43)	1120 (129)

Table 3 The failure properties for test beams from A73 (5°C, 0.01mm/s)

Section	Number of specimens	Max stress (MPa)	Strain at max load	Initial modulus (MPa)	Energy until max load (mJ)	Energy until deflection-1.5mm (mJ)
A73-R	3	3.09	6.7E-03	1.966	284	618
A73-P1	2	2.68	5.5E-03	1.580	202	504
A73-P2	1	2.22	8.3E-03	1.217	265	464
A73-P3	3	3.29	5.2E-03	2.347	233	610

It is important to mention that these values can be used as a first estimate in case one wants to compare the actual situation of other sections with these sections. From the stiffness tests it also becomes clear that the test sections are still in good condition, also over the height of the layer.

4.5 Ravelling (RSAT) results [11, 12]

The results of the RSAT for A50 are given in Table 4. Three tests were done for each section, except the treated section A50-B with two tests. A large variation in individual results of cumulative loss of stones can be observed. Average values of cumulative loss of stones were calculated. The treated sections (A50-E, A50-B and A50-H) show less cumulative loss of stones than the reference sections (A50-Reference). So it seems that the treated sections have better ravelling resistance. More test results are needed to investigate the ravelling behaviour of porous asphalt with the RSAT method. However, in the Netherlands a lot of experience has been gained with this test method with very good results that compare very well with performance in the field have been reported.

Table 4 Results of RSAT for the specimens from A50

Section	A50-Reference			A50-E			A50-B		A50-H		
Total test time (hour)	24	24	24	24	24	24	24	24	24	24	24
Cumulative loss of stone (g)	0.98	3.07	6.32	5.53	0.61	0.09	1.62	3.11	0.57	0.47	2.14
Average cumulative (g)	3.46			2.08			2.37		1.06		

4.6 FTIR results [5, 10]

The IR spectra of binder samples are used to investigate the chemical influence of the new binder in the porous asphalt. On one hand, the special absorption peaks of new binder in the IR spectra may offer evidence of existence and/or absence of new binder in the porous asphalt at different depths. Also the change of degree in aging of the binder may indicate the influence of the new binder, compared to the reference. Figure 13 shows examples of the FTIR spectrum from different sections.

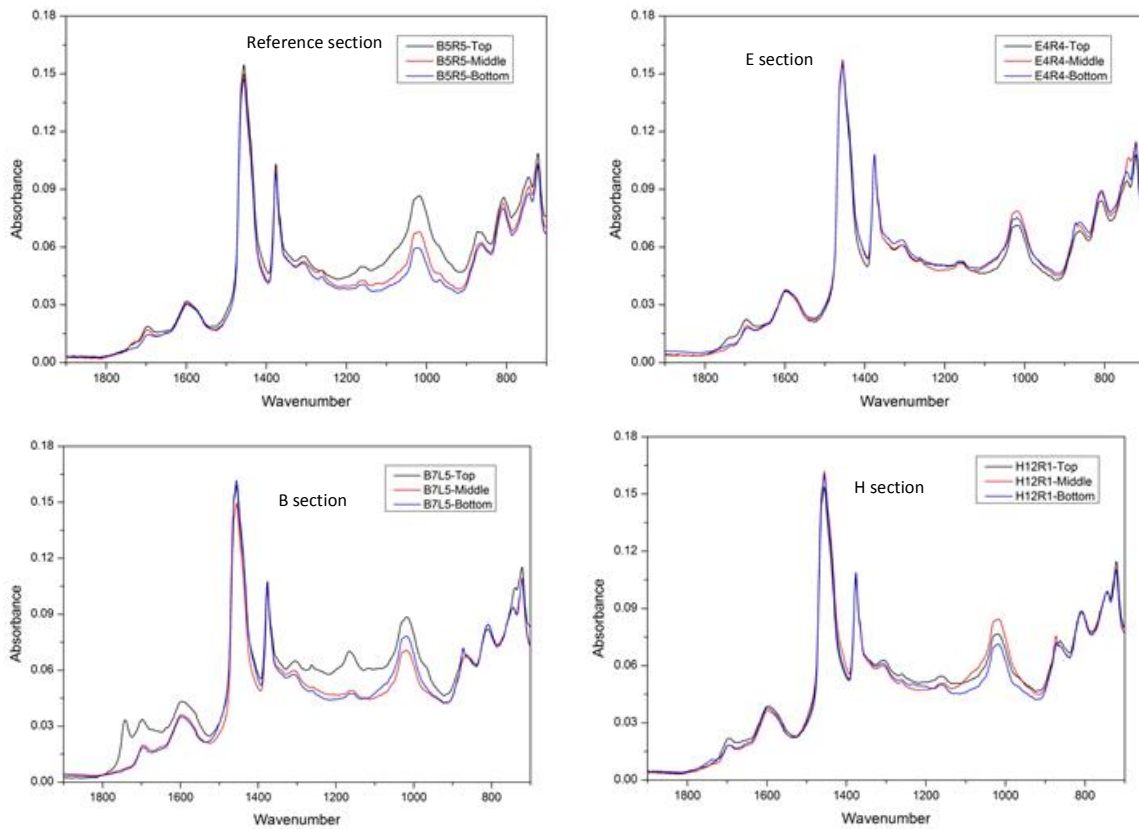


Fig 13. Examples of FTIR spectrum from reference section, E, B and H sections

The increase of the absorption peaks at $1710\text{-}1685\text{ cm}^{-1}$ (ketones C=O) and $1082\text{-}980\text{ cm}^{-1}$ (sulfoxides S=O) in the IR spectra of binder samples from all sections indicate the aging of bitumen in porous asphalt layer. No special absorbance peak in the IR spectra of the recovered bitumen could be detected, which only belongs to the spectrum of the new binder of the E and H section. Two special absorbance peaks could be detected at 1743 cm^{-1} and 1697 cm^{-1} in the IR spectrum of the binder sample recovered from the top part of the B section, which is related to the binder product of the B section. It shows that the new binder B can be detected in the top part of the porous asphalt surface layer with FTIR. In order to quantify the effect of the LVO product, an Ico index (peak of ketones C=O) was calculated shown as follows,

$$I_{co} = \frac{\text{area around } 1700\text{cm}^{-1}}{\text{area around } 2920\text{cm}^{-1} + \text{area around } 2851\text{cm}^{-1}}$$

As shown in Figure 14 the Ico index indicates that the aging decreases from the top to the bottom part of the porous asphalt layer. It means that the aging of the bitumen is higher at the surface of the porous asphalt layer.

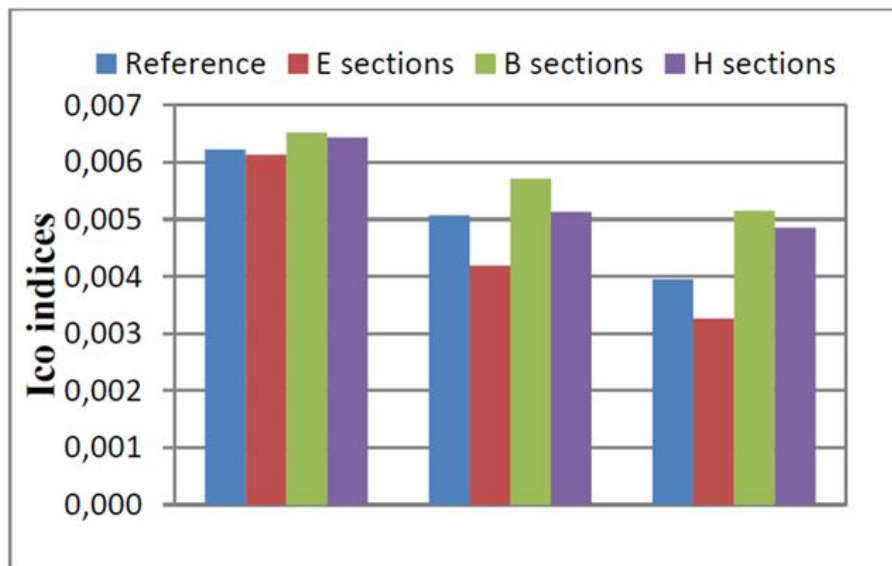


Figure 14. Development of Ico index for reference section, E, B and H sections

4.7 Discussion

Based on the CT scans of 150 mm cores it can be seen that even smaller test sections show quite some variability. Conclusions should be seen in relation to the inhomogeneity of the field trials.

With nanotom scans it can be shown clearly if there is new binder added to the material. It is not possible with this method to determine if there was diffusion in the aged mortar from the rejuvenating component in the binder. For two products it could be shown that new binder was added. This was not possible to show for one of the products. The two products with new binder showed very different distributions. One binder was purely observed in the surface (hot applied binder), not deeper than 10 mm. The other binder could be found over the whole height (emulsion with extra application action).

Interesting is to see that the E binder could not be found. This could give an indication that this binder contains a strong rejuvenator component.

From the nano indentation tests it could be seen that the mean value of the stiffness of the mortar in the treated sections was always lower than in the reference sections. This could be an important indication that all three new binders make the mortar more flexible. As a consequence one could expect in this case that all three binders are able to more or less diffuse partly in the mortar of the porous layer. An important feature from the nano indentation is that at the place of the nano indentation also excellent microscopic pictures are given from the computer.

The microscopic pictures confirm the impression that the mortar bridges between the stones are really strengthened by the addition of the new binders. Certain voids are filled, cracks are filled where possible and for the sections with B and H binders clearly extra binder can be observed.

The bending tests give a good indication of the bending stiffness of the porous layer over the height by testing in both directions in tension/compression. The mean values of the stiffness surface down were always lower than the stiffness values surface up. The tensile strength with surface down test gave similar values for all the test sections 5 years after construction. No significant differences could be observed between the reference sections and the treated sections. This is probably an indication that the reference section was still in good shape at the time of the treatment.

The FTIR analyses showed based of the Ico index, that the binder in the reference sections were more severely aged in the top part than in the bottom part of the porous layer. This result confirms that it is probably very important to treat the mortar in the top part of the layer with new binder, which has also

the ability to rejuvenate the aged binder in the mortar. In some cases it was observed that probably some filler was recovered with the binder. If the binder can be recovered fully more conclusions can be drawn from the FTIR test, because of the influence of the filler.

The analysis from both the microscope pictures and the nano CT scans lead to the same observations: for the sections with the E binder no new binder can be detected; for the sections with the B binder only in the top part of the layer new binder can be observed; for the sections with the H binder new binder can be observed over the whole height of the porous layer.

The results of the RSAT tests are in line with the results from the nano indentation, the nano CT scans and the microscopic pictures. It is important to realize that the microscopic pictures were a very important qualitative aid to support the test results, but that for future testing it is probably good enough to make slices for nano indentation and combine the pictures from the nano indenter microscope with the indentations.

Based on the relatively low number of test results it is impossible at the moment to get a fully statistically supported view on the use of these new binders. Especially the non homogeneity over the length of a test section of the voids content makes it very difficult at this moment to make conclusions. More results are needed for a sound statistical analysis.

In this project a number of new procedures are developed: procedures to produce slices for nano indentation and microscopy, a special three point bending test on the porous layer was developed, a recovery method was developed to test binder at several places in the layer from the mortar with FTIR analysis, a very special nano indentation test at a very low temperature of -20°C.

The usefulness of the several tests is summarised in table 5.

Table 5. Summary of the effect measured with the different tests for the three new binders.

Subject	Test	New binder		
		E (emulsion)	B (hot binder)	H (emulsion)
Detection new binder	Siemens CT	-	-	-
	Nano CT	-	yes	yes
	Nano indentation	yes	yes	yes
	Microscopy	-	yes	yes
	FTIR	-	yes	-
	GPC	yes	yes	yes
Rejuvenating old binder	Nano indentation	yes	yes	yes
Repair bridges	Nano indentation	Yes	Yes	Yes
	Microscopy	Yes	Yes	Yes
	Nano CT	yes	yes	yes
Depth of new binder	Nanotom	-	Yes	Yes
	Nano indentation	yes	Yes	Yes
	Microscopy	-	yes	yes
Improvement resistance to ravelling	RSAT	Yes	yes	yes
	Nano indentation	yes	yes	yes
	Bending test	-	-	-

5. CONCLUSIONS AND RECOMMENDATIONS

5.1 Conclusions

A set of tests were developed to investigate the effect of adding new binder as a preventive maintenance measure on porous surfacings. Both volumetric, mechanical and chemical characterisation was done of the treatment.

The distribution and effect of the three binders could well be compared with the test matrix used.

The three products which were all applied in a different way, have different interaction with the porous layer. All three improve the bridging and flexibility in the top of the layer. Binder E could hardly be detected via volumetric observations. Binder B was only observed in the top part of the layer. Binder E was observed over the whole height of the porous layer.

It was shown with FTIR that the binder in the top of the porous layer was more severely aged than the binder deeper in the layer. This stresses the importance of at least adding enough rejuvenating binder in the top part of the porous layer.

In this research a realistic ravelling test (RSAT) was compared with a number of fundamental tests and the rating was quite similar. This looks very promising for linking the developed test to ravelling in the field.

The developed tests can be used in the development of an acceptance protocol, before a new binder is allowed for application.

Due to the variability in the composition of the porous layer (based on variation in voids content) the number of tests in the research was not large enough to give statistical evidence of differences.

5.2 Recommendations

Based on the results it was proposed to use the three products tested on large scale applications.

It is recommended to combine large scale application with a statistical interpretation of some of the tests that could be done during the upscaling without major cost, with the aim to show the difference between the reference sections and the treated sections in time.

It is recommended to develop a trigger value for the quality of the porous layer before treatment is started.

REFERENCES

- [1] Wim Verwaal, Yuan Zhang, Feng Chen. **Field trial A50: Year 0 Results of CT Scans**. Report 7-11-185-1. Delft University of Technology. 2011
- [2] Erik Schlangen, Quantao Liu. **Field trial A50: Year 0 Results of Optical Microscope Analysis**. Report 7-11-185-2. Delft University of Technology. 2011
- [3] Erik Schlangen, Quantao Liu. **Field trial A50: Year 0 Results of Nano Indentation Test**. Report 7-11-185-3. Delft University of Technology. 2011
- [4] Marco Poot, Yuan Zhang, Feng Chen. **Field trial A50: Year 0 Bending Beam Test**. Report 7-11-185-4. Delft University of Technology. 2011
- [5] Martin van de Ven, Yuan Zhang, Feng Chen. **Field trial A50: Year 0 FTIR Test**. Report 7-11-185-5. Delft University of Technology. 2011
- [6] Wim Verwaal, Yuan Zhang. **Field trial A73: Year 0 Results of CT Scans**. Report 7-11-185-7. Delft University of Technology. 2011
- [7] Yuan Zhang, Quantao Liu. **Field trial A73: Year 0 Results of Optical Microscope Analysis**. Report 7-11-185-8. Delft University of Technology. 2011
- [8] Yuan Zhang, Quantao Liu. **Field trial A73: Year 0 Results of Nano Indentation Test**. Report 7-11-185-9. Delft University of Technology. 2011
- [9] Yuan Zhang, Marco Poot. **Field trial A73: Year 0 Bending Beam Test**. Report 7-11-185-10. Delft University of Technology. 2011
- [10] Jian Qiu, Yuan Zhang, Martin van de Ven. **Field trial A73: Year 0 FTIR Test**. Report 7-11-185-11. Delft University of Technology. 2011
- [11] Yuan Zhang, M.F.C. van de Ven, A.A.A. Molenaar, S. Wu. **Increasing the service life of Porous Asphalt with rejuvenators**. SUSCOM conference, Wuhan, China. 2012
- [12] Y. Zhang, M.F.C. van de Ven, A.A.A. Molenaar, M.F. Woldekidan, S. Wu. **Mechanical Properties of Porous Asphalt Concrete with Rejuvenators**. BCRRRA conference, Trondheim, Norway. 2013

Appendix 1. Volumetrics

A1..1 CT scans [1, 6]

Two CT scanners [1,6] were used in this research. Firstly all 150mm cores were scanned in the Siemens CT- SOMATOM Plus4 Volume Zoom medical scanner to get information on the volumetric composition of all cores. The Siemens scanner is shown in figure A1a. Slices at distance of 1 mm were scanned over the height with a resolution of 0.3mm. An example is given in Figure A1b. After that small cores with 40 mm diameter were taken from the 150 mm cores and these were scanned in the Nano CT-scanner.

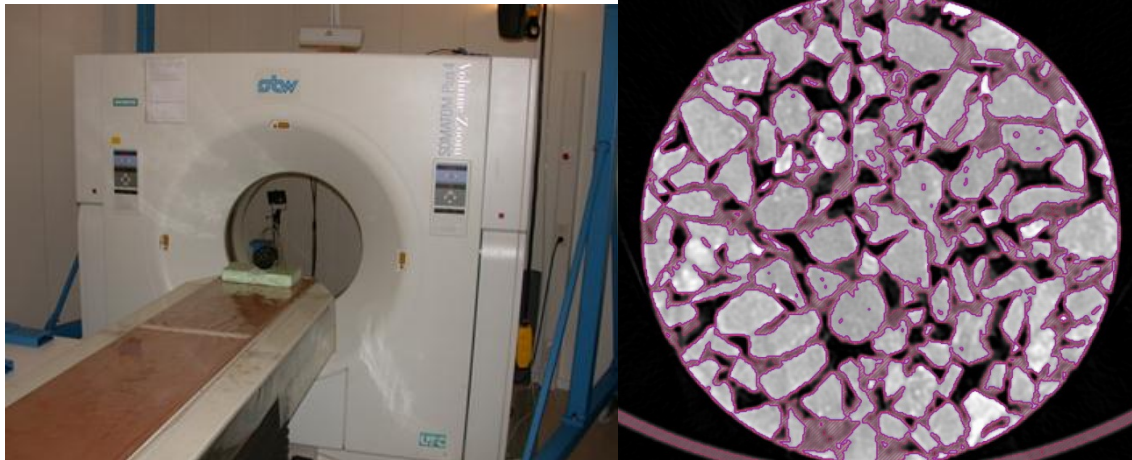


Figure A1a: Siemens medical scanner,

A1b: Slice of a SLPA core

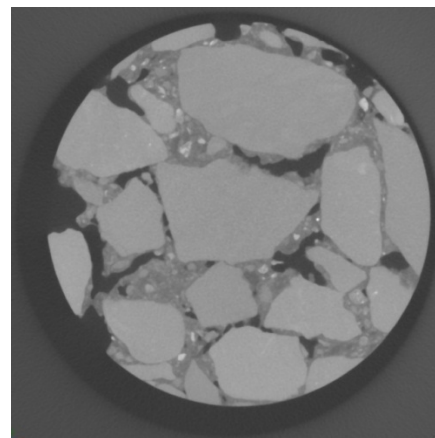
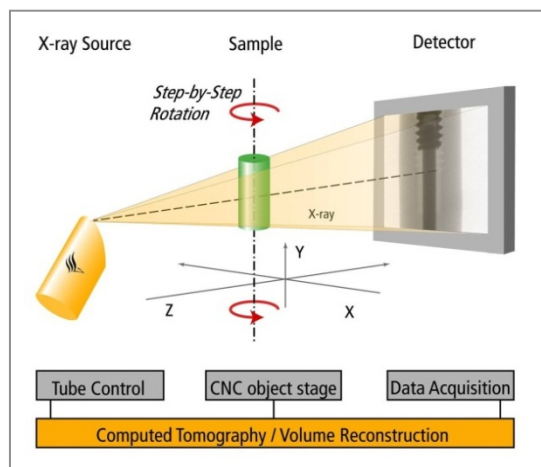


Fig A2a: A schematic diagram of the phoenix Nanotom, A2b: Typical cross sections near the top of a core sample with three components (voids, mortar, stone)

Figure A1b shows a slice with the segmentation boundaries of a SLPA core, a black colour represents the voids, the dashed part is the mortar and the grey colour is the aggregate. In order to get high resolution scans, the Phoenix Nanotom scanner is used to determine the exact mix composition at micro level. Scans were made with a slice distance and resolution in the slice of 0.04 mm in top parts of the small cores with a diameter of 40 mm. A schematic diagram of the Phoenix Nanotom is given in figure A2a. Digital geometry processing is used to generate a three-dimensional image of the inside of an object from a large series of two-dimensional X-ray images taken around a single axis of rotation. The different

composition in the sample presents different grayscale values in two-dimensional X-ray images as shown in figure A2b.

A.1.2 Thin section optical microscopy [2, 6]

From the small cores for the Nano CT scans, slices are produced for microscopic analysis of the bridges between the stone skeleton [2.6]. The microscopic pictures will allow the observation of the quality of bitumen coating on the aggregates, but also the location of the new binder on the bridges between the stones. The interface formed between bitumen and stones and the location of at least part of the new binder can be detected in such a way. Figure A3 shows a picture of the Polarizing Microscope in the Microlab of TUDelft used for the study. The incident and transmitted light is used in the microscope. The magnification of the microscope can reach up to 600x.



Figure A3. Picture of the Polarizing Microscope (LEITZ DM RXP) in the Microlab of TUDelft

In order to clearly observe the bitumen-aggregate interfaces the samples were polished. The polishing operation is delicate as it can irreversibly damage the interface by taking off the binder and smearing the binder in cracks. The polishing action can locally increase the temperature due to friction from the mechanical action and can take away the softened bitumen from the interface. So it is important to develop the right procedure to polish the samples.

In order to produce slices from the small cores, the voids in the cores must first be filled with the epoxy resin to prevent changing the configuration during the production process of the slices. During the sawing and the polishing process special care will be taken to make sure that no bitumen is removed.

First of all, the 40 mm diameter cores from the Nano CT scans will be saturated with epoxy resin under vacuum for 1 hour. With the vacuum it is possible to fill pores and cracks with epoxy. The epoxy will serve as support for the bitumen during the sawing and polishing operation but it can also help to prevent removal of the binder. Once the resin is hardened, the specimens can be sawn to a dimension of about 40×50×5 mm³ so they can be more or less placed on the sample holder of the microscope. During this sawing action very cold water (ice water) should be used to prevent smearing of the bitumen. The specimens are then ready for polishing.



a) Sawing and burnishing machine



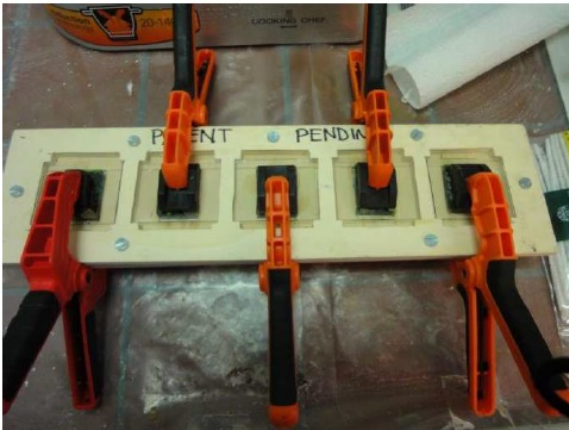
b) The sample saturated with epoxy resin



c) Polishing paper



d) Burnishing the sample



e) Glue sample to the object glass



f) Thin sections for microscope test

Figure A4. Pictures of the preparation of the thin sections for the microscope test

To reduce the thickness of the slice to 25 micrometers, they were polished successively on abrasive silicon carbide paper of 500, 1200 and 4000 grid under very cold water at high flow. The polishing duration with abrasive paper was quite short taking into account the big size of the polishing grains which could induce damages in the specimens. After that the burnishing machine was used to burnish

the slices. After polishing the specimens were cleaned ultrasonically in a water bath at room temperature. The pictures of the preparation of the thin sections are shown in figure A4.

For each thin section, 8 observation points were selected to take pictures under the microscope. The selected observation points were taken at the top, middle and bottom part of the core. Some of the observation points are at the bridge between two stones. Some are from the surface of a stone or from the mortar. In the reports [2, 6] the observation points are labeled in the picture of every thin section.

Appendix.2 Development of Mechanical properties

A.2.1 Nano indentation [3,8]

Nano indentation technology has become important and popular for measuring the mechanical properties of materials at nanometer scale. It's a fairly mature technique which uses the recorded depth of penetration of an indenter into the specimen along with the measured applied load to determine the area of contact and hence the hardness of the test specimen. It is also possible to calculate a stiffness value. The nano indentation test is used to study the bridges in the top part of the porous asphalt layer. The hypothesis is that the new binder and its influence on the modulus and hardness of the aged mortar by diffusion can be measured over the bridge area between two stones.

From the small cores for the nano CT scans, blocks were produced for nano indentation tests on the bridges between the stone skeleton. The blocks were produced in such a way that the area for the indentation presents the vertically scanned zone with the nano CT scanner. In this way these results can be linked together. A schematic vertical view of a bridge between two stones at the surface of a PA layer is shown in figure A5.

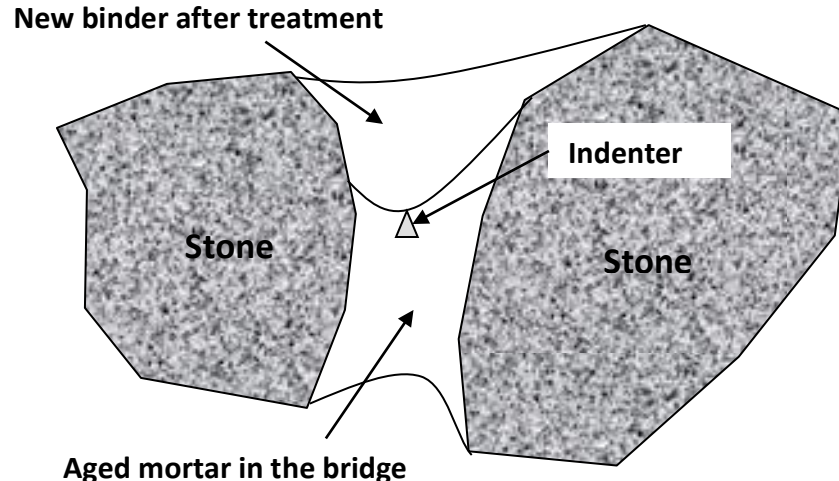


Figure A5. Schematic vertical view of a bridge between two stones for nano indentation test.

A typical indentation curve is shown in figure A6. The recorded load of the indenter increases until the indenter reaches to the given maximum displacement. Then the maximum load is held for a certain period. After that, the applied load is removed to let the indenter go back to the initial position. Through plotting of the unloading data, the stiffness can be deduced. It is the slope of the tangent line to the unloading curve at the maximum loading point. In addition to the stiffness, the hardness can be obtained from the maximum load divided by the contact area. In order to clearly observe the bitumen-aggregate interfaces, the samples were polished.

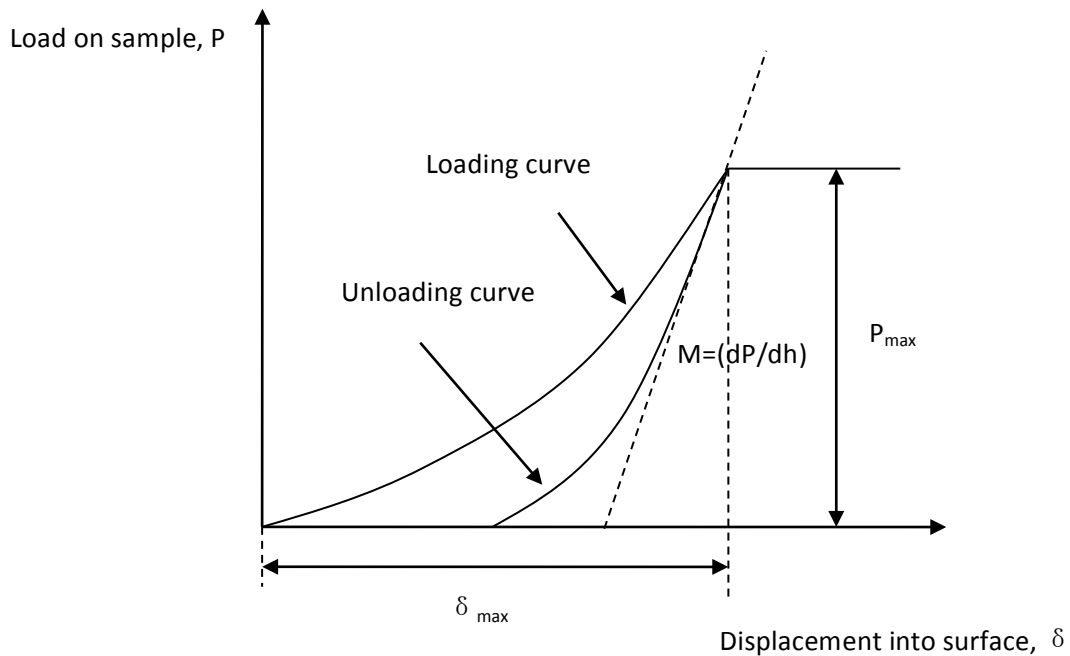


Figure A6. A typical indentation curve of load on sample vs. displacement into surface

A similar process was followed as for the preparation of the microscope slices shown in figure A4. During the sawing and the polishing process special care was taken to make sure that no bitumen was removed. The polishing operation is delicate as it can irreversibly damage the interface by taking off the binder and smear the binder into the cracks. The polishing action can locally increase the temperature due to friction from the mechanical action and can take away the softened bitumen from the interface. So it is important to develop the right procedure to polish the samples.

Delft University of Technology has a Nano Indenter with CSM-option (Continuous Stiffness Measurement) and cooling-heating stage (range $-40/+200$ °C). Also included is a Nano-vision system to perform surface scanning. Figure A7 shows a picture of the Nano Indenter MTS G200 in the Microlab. It has a displacement resolution of 0.01 nm and a load resolution of 50 nN. The maximum indentation depth is 500 μm and maximum load 500 mN.

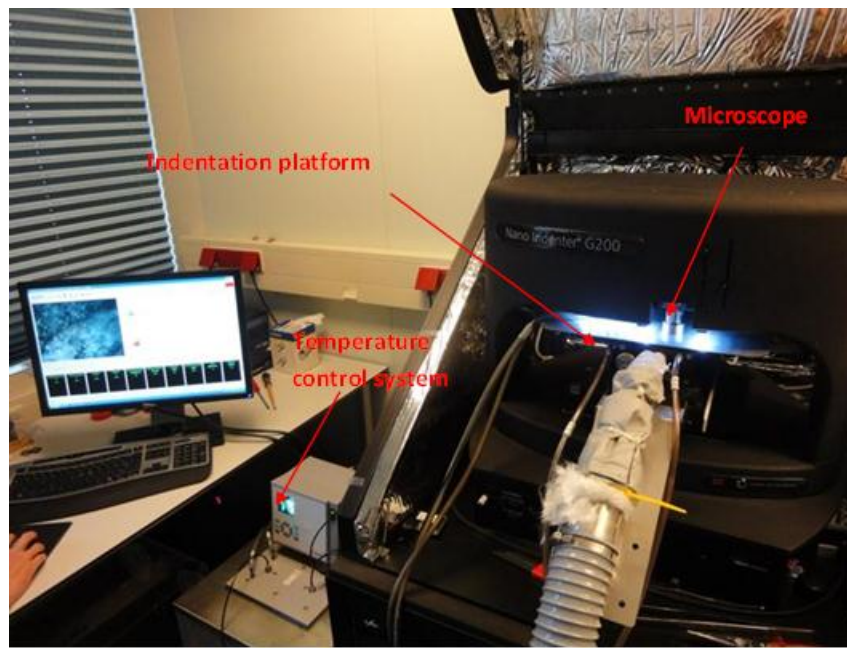


Figure A7. Picture of the Nano Indenter MTS G200 in the Microlab of TU Delft

In this research, the test program of G-Series Basic Hardness and Modulus at a Depth was used, which means that the indenter is penetrating into the surface of the sample to a given depth. The three phases during the testing were:

- The indenter penetrates into the surface with 5 nm/s until the depth of 1000 nm;
- The maximum load on the indenter is held for 1 second;
- The applied load on the indenter is removed. The indenter is rebounded from the surface of sample with the load recorded.

The tests were performed at a very low temperature of -20°C to avoid the problems caused by the visco-elastic properties of the bituminous binder. Microscope pictures were taken at each test region. In each test region, at least 10 indentation points were set in the Continuous Stiffness Measurement option system. The location of indentation points only changed in vertical direction over the height of the PA layer. The distance between two neighbouring points was $25\ \mu\text{m}$. The location of indentation points are marked in the pictures of test regions.

A.2.2 Bending Beam test [4.9]

A three point bending test was developed to measure the stiffness of porous asphalt beams [4]. The beams were subjected to a haversine loading with a frequency sweep between 0.1 and 4 Hz at a temperature of 5°C . Applied loads for SLPA beams and TLPA beams are 100 N and 60 N, respectively.

The results of the bending stiffness E are corrected with a shift factor κ as shown in Equation (1) for the shear deflection. Two shift factors obtained from the SLPA beam model and TLPA beam model are used to calculate the bending stiffness.

$$E = k \cdot \frac{PL^3}{48 \cdot \delta_{max} I} \quad (1)$$

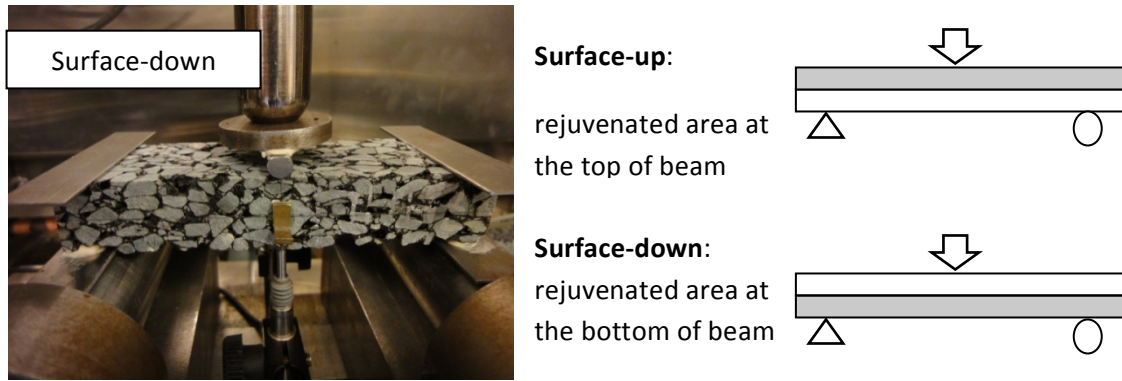


Figure A8. Picture of the three-point bending test and a schematic diagram of the two test modes

As shown in figure A8, two test modes were used to measure the stiffness in the bending test. Due to the penetration depth of rejuvenators, the upper part of the beam (in the as-built orientation) is the rejuvenated area. In the surface-up mode, the rejuvenated area is located at the top and under compression. In the surface-down mode, the rejuvenated area is located at the bottom and under tension.

To determine the influence of the shear deflection on the stiffness a first analysis was done to quantify the influence caused by the dimensions of beams. In this analysis a homogeneous elastic beam FE model was used and the maximum deflection obtained with ABAQUS was compared with the results of analytical solutions. Equation 1 was used for the analytical solution. Using the regression function, shift factors for SLPA beam model and TLPA beam model were determined. As shown in figure A9, the shift factor of the SLPA beam mode is higher than the TLPA beam model.

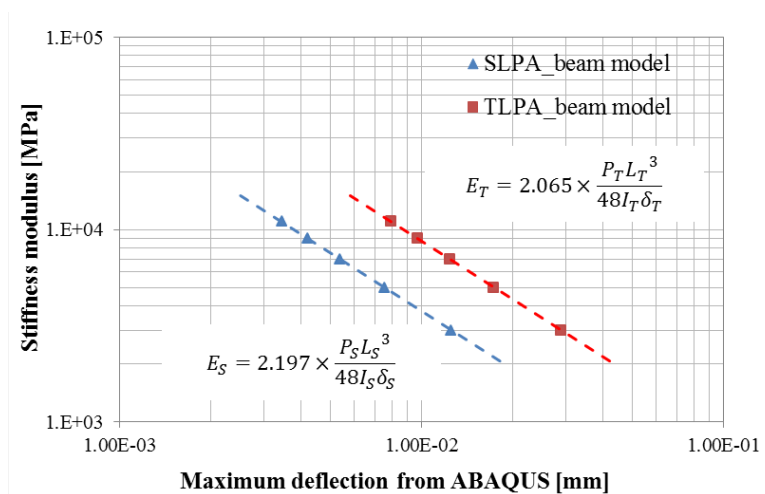


Figure A9: Stiffness modulus vs. the deflection with shift factors

To study the influence of the new binder and rejuvenated zones in the mortar detailed FE models were build in ABAQUS. Results are reported in [12] and not discussed here.

A.2.3 Rotating Surface Abrasion Test (RSAT) [11, 12]

The resistance to ravelling was measured with a test method developed by Dutch contractor Heijmans, the Rotating Surface Abrasion Test [11]. In the standard test, an octagonal slab of 50 cm in diameter is charged by a wheel with a solid rubber tire that is moved back and forth (3607 times per hour). The vertically loaded wheel (contact stress of 0.6 MPa) is tilted (33.7°) in the direction of back and forth movement so that the horizontal forces occur on the surface. The entire surface of the test plate is substantially uniformly loaded by rotating the test slab during the test (496 circles per hour). During the 24 hours test at a temperature of 20°C, the loss of material from the surface is collected continuously with a vacuum cleaner. The mass consisting of stones with a grain diameter of more than 2 mm is reported as ravelling damage. Because we were not allowed to take slabs from the tests sections in the field in this research, three cores with a diameter of 150 mm from the road surface were glued in a multiplex slab with the same shape as the standard test slab. The rest of the test conditions remained the same. A schematic of the RSAT test and a picture of the test specimens are given in figure. A10

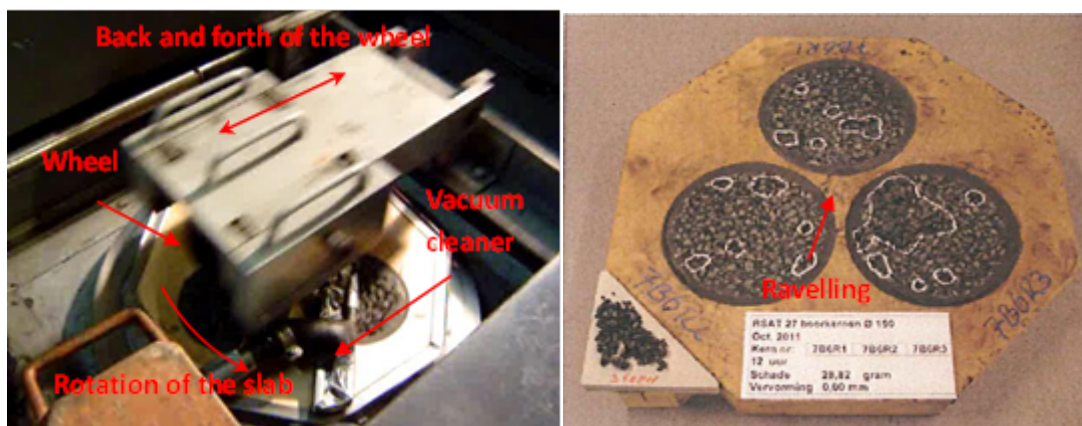


Figure A10. Rotating Surface Abrasion Test (left) and a picture of the specimens after RSAT from the test section of A73 (right)

Appendix 3 Chemical analysis

A.3.1 Recovery of binder for chemical composition [5, 10]

The broken beams after the bending test were used to get the binder samples for the FTIR test. The beams were cut into three parts: top, middle and bottom part. It was not possible to use the standard bitumen recovery method. Therefore, a special recovery method was developed in this research.

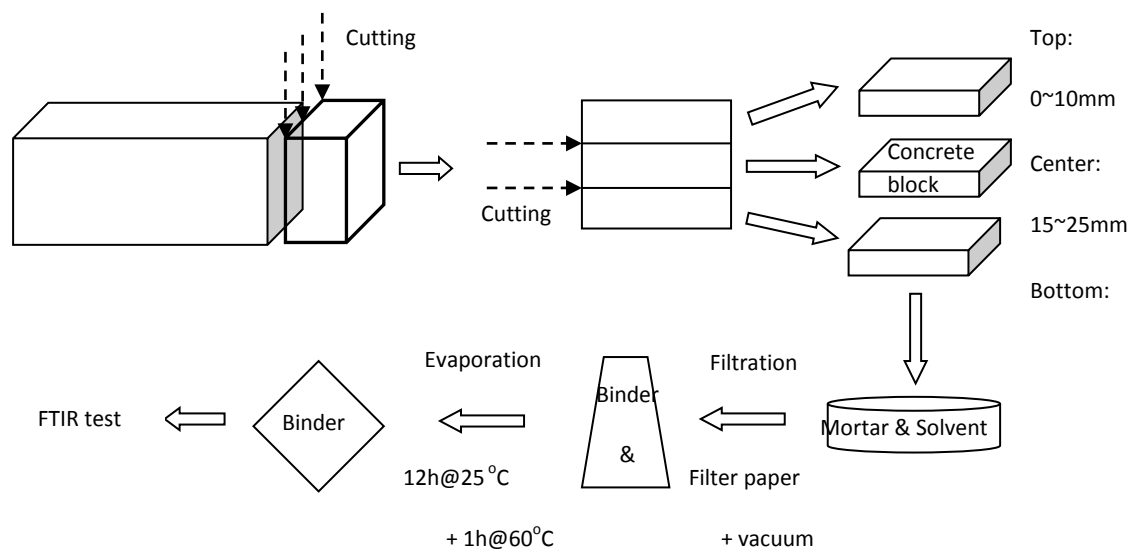


Figure A11. Schematic diagram of preparation method for the binder samples

As shown in figure A11 the broken beams were first sawn into three blocks, top part (at depth of 0-10 mm), middle part (depth of 15-25 mm) and bottom part (depth of 30-40 mm). From these blocks a small quantity of mortar was taken. Then the mortar was dissolved in a cold solvent (Dichloromethane, CH_2Cl_2). A filtration device was used to separate the minerals from the binder solution under vacuum, for which filter paper with sieve sizes of 5×10^{-6} m and 1.6×10^{-6} m were used. After the solvent was evaporated in the air for 12 hours and in the oven at 60°C for 1 hour, the binder was recovered from the solution. The process of the preparation for the binder samples is showed in Figure A12.

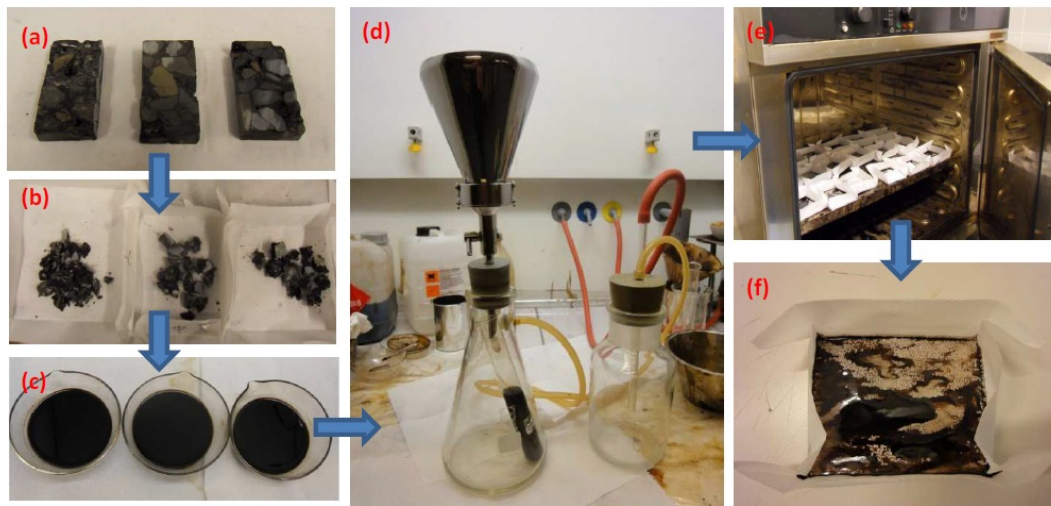


Figure A12. The process of the preparation for the binder samples: (a) porous asphalt concrete blocks; (b) the mortar from blocks; (c) the binder solution; (d) filtration device with vacuum; (e) evaporation in oven; (f) the binder sample

A.3.2. FTIR analysis [5, 10]

The binder samples were tested with the Perkin Elmer Spectrum 100 Series FT-IR spectrometer using ATR FT-IR spectroscopy. The spectrometer with a resolution of 4 cm^{-1} is showed in figure A13. A typical FTIR spectrum of virgin and aged bitumen is shown in figure A13.

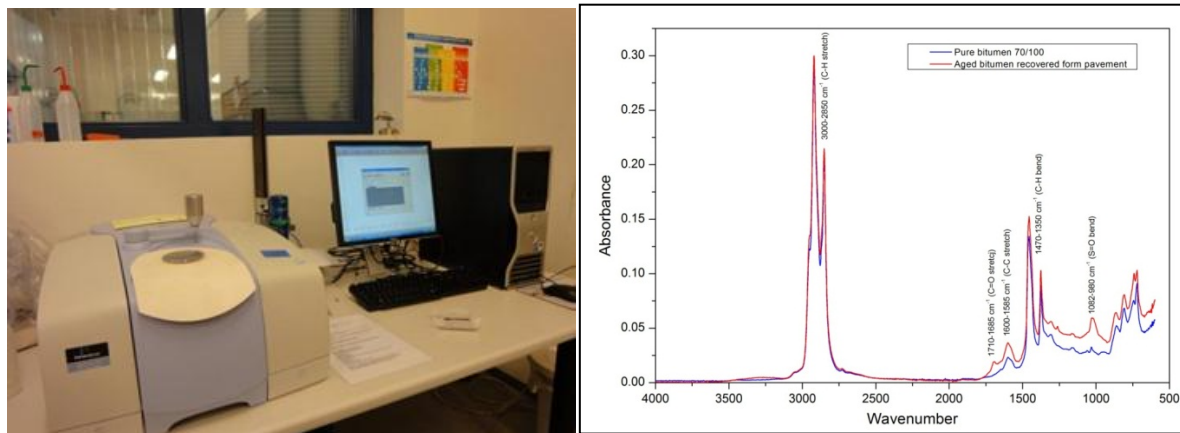


Figure A13. The PerkinElmer Spectrum 100 Series FT-IR spectrometer and typical IR spectra of pure bitumen and aged bitumen

The absorption peaks at $3000\text{--}2850\text{ cm}^{-1}$ and $1470\text{--}1350\text{ cm}^{-1}$ represent functional groups of C-H stretch and C-H bands respectively. They are characterized with approximate same strong peaks in the IR spectra of pure and aged bitumen. However, for aged bitumen, the absorption peaks at $1710\text{--}1685\text{ cm}^{-1}$ (ketones C=O) and $1082\text{--}980\text{ cm}^{-1}$ (sulfoxides S=O) are the two obvious characteristic bands due to the aging. The height of these peaks and the area under these peaks can be used as indicators of aging of the bitumen.